Research article

Shulei Li, Lidan Zhou, Mingcheng Panmai, Jin Xiang and Sheng Lan*

Magnetic plasmons induced in a dielectric-metal heterostructure by optical magnetism

https://doi.org/10.1515/nanoph-2021-0146
Received April 7, 2021; accepted June 25, 2021;
published online July 8, 2021

Abstract: We investigate numerically and experimentally the optical properties of the transverse electric (TE) waves supported by a dielectric-metal heterostructure. They are considered as the counterparts of the surface plasmon polaritons (i.e., the transverse magnetic (TM) waves) which have been extensively studied in the last several decades. We show that TE waves with resonant wavelengths in the visible light spectrum can be excited in a dielectric-metal heterostructure when the optical thickness of the dielectric layer exceeds a critical value. We reveal that the electric and magnetic field distributions for the TE waves are spatially separated, leading to higher quality factors or narrow linewidths as compared with the TM waves. We calculate the thickness, refractive index and incidence angle dispersion relations for the TE waves supported by a dielectric-metal heterostructure. In experiments, we observe optical resonances with linewidths as narrow as ~10 nm in the reflection or scattering spectra of the TE waves excited in a Si_3N_4/Ag heterostructure. Finally, we demonstrate the applications of the lowest-order TE wave excited in a Si_3N_4/Ag heterostructure in optical display with good chromaticity and optical sensing with high sensitivity.

Keywords: dielectric-metal heterostructure; optical display; optical sensing; surface plasmon polariton; transverse electric wave; transverse magnetic wave.

1 Introduction

Surface plasmon polaritons (SPPs), which is a transverse magnetic (TM) wave (i.e., $\mathbf{k}\cdot\mathbf{H} = 0$ and $\mathbf{k}\cdot\mathbf{E} \neq 0$) propagating on the surface of a metal film, have received intensive and extensive studies since 1980s [1–3]. Owing to the strong localization of electric field achieved on the surface of the metal, SPPs has been exploited to construct plasmonic devices of different functionalities [4], such as waveguides [5, 6], sensors [7–10], and spacers [11–13] etc. However, many practical applications of SPPs are limited by their large damping rates, which are manifested in the broad linewidths of SPPs. In principle, the large loss of SPPs originates from the collective oscillation of electrons driven by the longitudinal electric field of SPPs [14–19]. Various scenarios have been proposed to overcome this disadvantage but a significant improvement remains a challenge [20–24].

In most cases, especially in practical applications, SPPs propagating on the surface of a bare metal film (or at the interface between air and a metal film) is taken into account. It has been known that such SPPs can only be excited by using *p*-polarized (or TM-polarized) light [25]. No SPPs will be generated if *s*-polarized (or TE-polarized) light is employed. The physical origin for this behavior is that a transverse electric (TE) wave is not supported by a bare metal surface (i.e., an air/metal interface). Different from the longitudinal electric field in SPPs, which can be generated by the collective oscillation of electrons in the metal film, the longitudinal magnetic field cannot be established on a bare metal surface. For this reason, the counterparts of SPPs, a TE wave (i.e., $\mathbf{k}\cdot\mathbf{E} = 0$ and $\mathbf{k}\cdot\mathbf{H} \neq 0$) propagating on the surface of

Shulei Li and Lidan Zhou contributed equally to this work.

***Corresponding author: Sheng Lan**, Guangdong Provincial Key Laboratory of Nanophotonic Functional Materials and Devices, School of Information and Optoelectronic Science and Engineering, South China Normal University, Guangzhou 510006, China, E-mail: slan@scnu.edu.cn
Shulei Li and Mingcheng Panmai, Guangdong Provincial Key Laboratory of Nanophotonic Functional Materials and Devices, School of Information and Optoelectronic Science and Engineering, South China Normal University, Guangzhou 510006, China. https://orcid.org/0000-0001-9346-3773 (S. Li)
Lidan Zhou, Guangdong Provincial Key Laboratory of Nanophotonic Functional Materials and Devices, School of Information and Optoelectronic Science and Engineering, South China Normal University, Guangzhou 510006, China; and State Key Laboratory of Optoelectronic Materials and Technologies and School of Electronics and Information Technology, Sun Yat-sen University, Guangzhou, China
Jin Xiang, Department of Electrical and Computer Engineering, University of Wisconsin–Madison, Madison, USA

a metal film has long been ignored for both fundamental properties and device applications.

In recent years, dielectric nanoparticles with high refractive indices in the visible to near infrared spectral range, such as silicon (Si) [26, 27], germanium (Ge) [28] and gallium arsenide (GaAs) [29], have attracted great interest because they are considered as building blocks (i.e., meta-atoms) for metasurfaces and metamaterials operating at optical frequencies. All-dielectric photonic devices with a variety of functionalities, which are constructed by using such high-index nanoparticles, have been successfully demonstrated [30, 31]. The recent studies on the scattering properties of Si nanoparticle placed on a thin metal film reveal that the coherent interaction between the electric dipole (ED) excited in the nanoparticle and its mirror image induced by the metal film leads to the formation of a magnetic dipole (MD) at the contact point between the nanoparticle and the metal film [32–35]. This behavior reminds us that the oscillating magnetic field necessary for the excitation of a TE wave can be realized by adding a thin dielectric layer on the metal film. Early in 2006, it was shown that specially arranged metal nanoparticles can support magnetic plasmon resonances in the optical spectral range, paving the way for the development of subwavelength negative index material [36]. Recently, the optical magnetism in planar metamaterial heterostructures has been systematically investigated. It was demonstrated that TE waves can be excited in multilayer dielectric-metal heterostructures composed of dielectric layers of silicon dioxide (SiO_2), titanium dioxide (TiO_2), Ge and silver (Ag) thin film by exploiting the so-called optical magnetism [37, 38]. In addition, the TE waves excited in a $SiC/Ge_3Sb_2Te_6$ heterostructure was also investigated [39], where $Ge_3Sb_2Te_6$ is a phase-change material. Apart from high-index dielectric materials, dielectric materials with moderate refractive indices and low optical loss in the visible light spectrum have also been extensively studied owing to their potential applications in the construction of nanoscale functional devices. A typical example is silicon nitride (Si_3N_4), which is considered as a promising material for making waveguides and resonators operating in the visible light spectrum. It has the advantages of large bandgap, wide transparency range, high thermal stability, chemical inertness, and good insulating properties [40, 41]. More importantly, the fabrication of Si_3N_4 nanoparticles and nanostructures is compatible with the current fabrication of Si chips. Very recently, nanogratings made of Si_3N_4 have been successfully exploited to realize hologram with continuous phase modulation [42].

In this article, we investigate both numerically and experimentally the TE waves propagating in a dielectric-metal heterostructure. We design a Si_3N_4/Ag heterostructure that supports both TM and TE waves spanning the visible to near infrared spectral range. It is revealed that the thickness of the dielectric layer must exceed a critical value in order to support the TE wave of the lowest order. More importantly, it is found that the damping rate of the lowest-order TE wave is reduced dramatically as compared with that of the TM wave because of the spatial separation of the electric and magnetic fields, leading to a narrow linewidth of ~10 nm. Finally, we demonstrate the application of such TE waves in high-quality optical display and highly sensitive optical sensing.

2 Results and discussion

As mentioned at the beginning, SPPs propagating at the interface between a dielectric (including air) and a metal can only be excited by using *p*-polarized light, as schematically shown in Figure 1A. Such a TM wave contains two electric field components (E_x and E_z) and one magnetic field component (H_y). The electric field parallel to the propagation direction (E_x) is correlated with the periodic oscillation of free electrons in the metal film. As the counterpart of the TM wave, the TE wave supported by a dielectric-metal heterostructure should contain one electric field component (E_y) and two magnetic field components (H_x and H_z). While a TM wave can be excited on the surface of a bare metal (i.e., at the interface between air and a metal film), such a TE wave does not exist because of the absence of an analytical solution to the Maxwell equation. From the viewpoint of optical magnetism, an MD can be created by exciting the ED in a dielectric block placed on a metal film. This phenomenon has been well studied by using the so-called mirror-image theory [32]. By enlarging the lateral dimensions of the dielectric block, one can create a periodically arranged magnetic dipole moments in a dielectric-metal heterostructure, exciting a TE wave with one electric component (E_y) and two magnetic components (H_x and H_z). As demonstrated in the following, the resonant wavelength of the lowest-order TE wave enters into the visible light spectrum when the optical thickness of the dielectric layer exceeds a critical value. In other words, an analytical solution to the Maxwell equation is present in the visible light spectrum when the optical thickness of the dielectric layer exceeds a critical value.

Now we examine a dielectric block (e.g., a Si_3N_4 cuboid) with a side length of d and a height of h placed on a thin metal film (e.g., Ag film with a thickness of 50 nm) supported by a SiO_2 substrate, as sketched in Figure 1B. The radiation spectra of two Si_3N_4 cuboids with d = 200 and

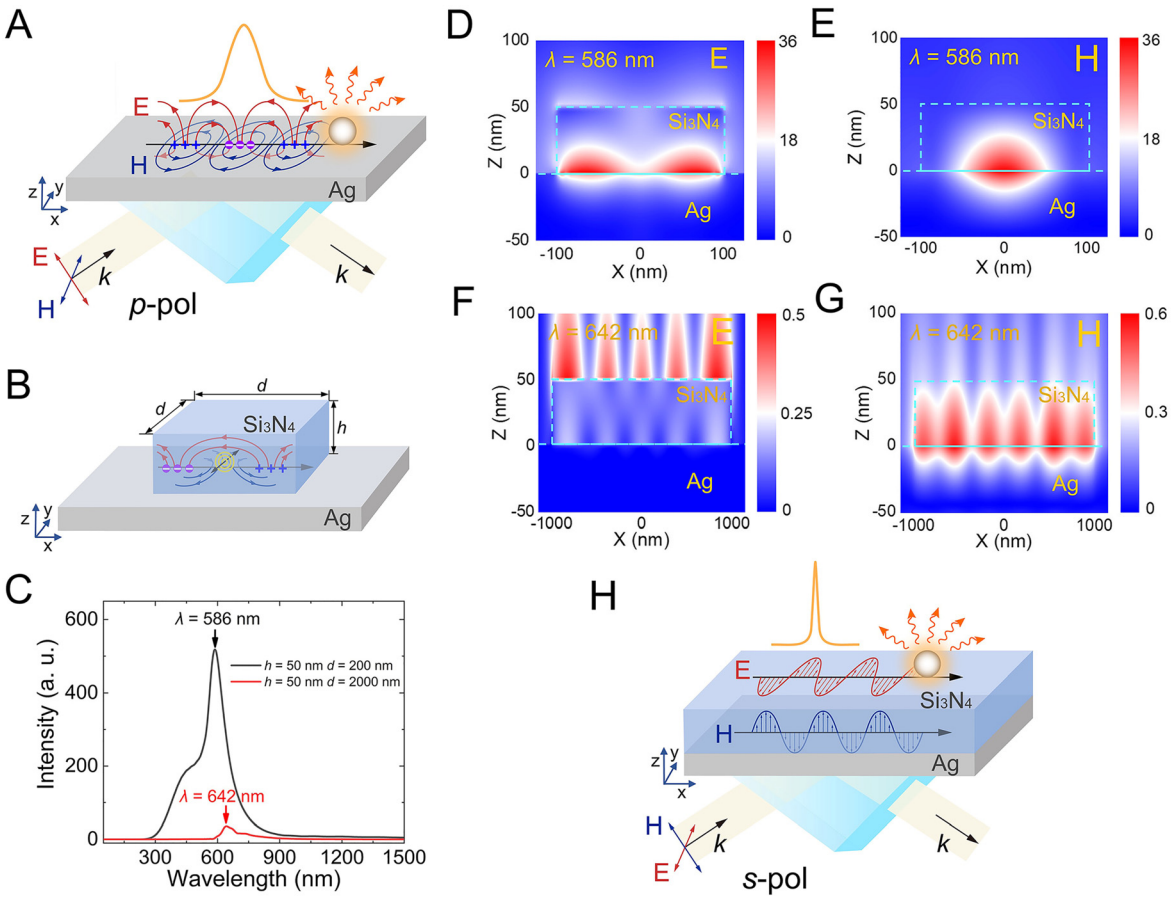

Figure 1: (A) Schematic showing the excitation of a TM wave (SPPs) on a bare metal surface by using *p*-polarized light. The TM wave can be scattered into free space by using a nanoparticle on the metal surface. (B) A Si_3N_4 cuboid placed on an Ag film. A horizontally oriented dipole source is used to excite the optical modes supported by the Si_3N_4 cuboid. (C) Radiation spectra calculated for two Si_3N_4 cuboids with d = 200 and 2000 nm, h = 50 nm, which are excited by the horizontally oriented dipole source. (D) and (E) Electric and magnetic field distributions calculated for a Si_3N_4 cuboid with d = 200 nm at λ = 584 nm. (F) and (G) Electric and magnetic field distributions calculated for a Si_3N_4 cuboid with d = 2000 nm at λ = 642 nm. (H) Excitation of a TE wave propagating in a dielectric-metal (Si_3N_4/Ag) heterostructure by using *s*-polarized light. The TE wave can be scattered into free space by using a nanoparticle on the metal surface.

2000 nm (h = 100 nm in both cases), which are excited by using horizontally oriented dipole sources placed in the Si_3N_4 cuboids, are shown in Figure 1C. If we examine the amplitudes of the electric and magnetic fields at the peaks of the radiation spectra of the two Si cuboids, which appear at ~586 and ~642 nm respectively, we can reveal the optical modes supported by the Si_3N_4/Ag hybrid structures, as shown in Figure 1D–G. In Figure 1D, one can see a standing wave localized at the interface between the Si_3N_4 cuboid and the Ag film for the small Si_3N_4 cuboid, creating a node in the electric field distribution. As a result, a strong localization of the magnetic field can be achieved at the bottom center of the Si_3N_4 cuboid, as shown in Figure 1E. Similar behavior is observed in the large Si_3N_4 cuboid, as shown in Figure 1F and G. Differently, the electric field is localized on the surface of the Si_3N_4 cuboid while the magnetic field is localized at the interface between the Si_3N_4 cuboid and the Ag film. It implies that optical magnetism could be created by introducing a dielectric layer with a sufficiently large thickness or refractive index on the surface of a metal film, forming a dielectric-metal heterostructure. In our case, it is expected that a periodic localization of magnetic field can be achieved in a Si_3N_4 layer (with infinite area) deposited on the Ag film. Therefore, the excitation of a TE wave propagating in the Si_3N_4/Ag heterostructure by using *s*-polarized light will become possible, as illustrated in Figure 1H.

Now we compare the electric and magnetic field distributions in the lowest-order TM and TE waves, as shown in Figure 2. For the TM wave, it can be seen that the electric and magnetic fields are mainly distributed in air with a decay length of more than 100 nm. Since they exhibit quite

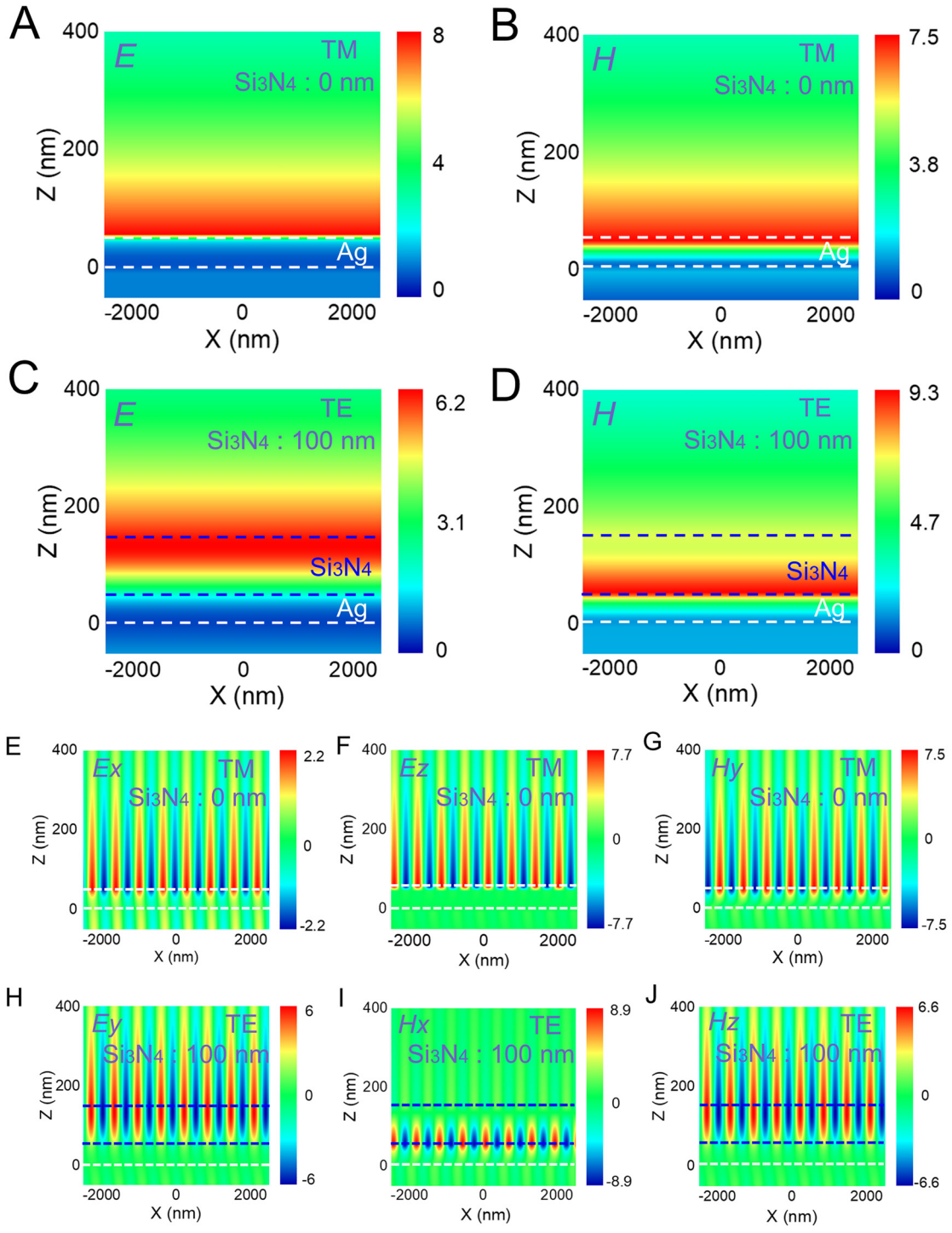

Figure 2: Electric and magnetic field distributions calculated for the lowest-order TM and TE waves.
Total electric field distribution in the XZ plane calculated for the TM (A) and TE (C) wave. The corresponding magnetic field distributions are shown in (B) and (D), respectively. (E) and (F) The E_x and E_z components for the TM wave. (G). The H_y component for the TM wave. (H) The E_y component for the TE wave. (I) and (J) The H_x and H_z components for the TE wave.

similar distributions, it is expected that the overlap between them is very large. In sharp contrast, a complete different behavior is observed for the TE wave. While the electric field is distributed on the top surface of the Si_3N_4 layer, the magnetic field is localized at the interface between the Si_3N_4 layer and the Ag film (or on the bottom

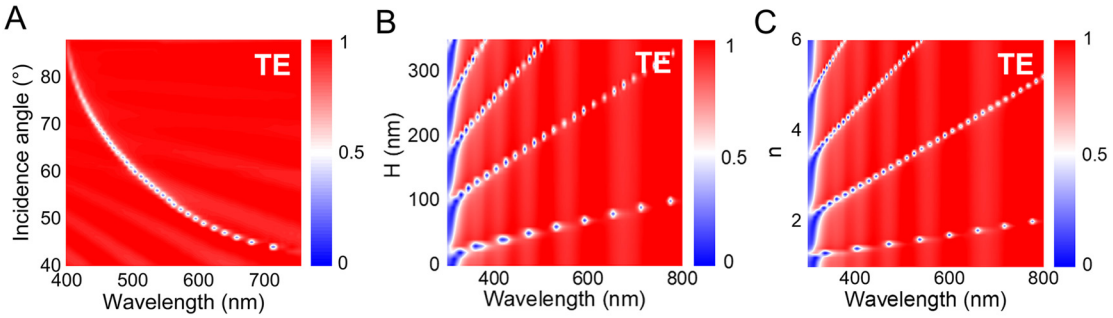

Figure 3: (A) Dependence of the resonant wavelength of the lowest-order TE wave on the incidence angle of the excitation *s*-polarized light calculated for a Si_3N_4/Ag heterostructure with h = 90 nm. (B) Thickness dispersion relations calculated for TE waves of different orders supported by Si_3N_4/Ag heterostructures with Si_3N_4 layers of different thicknesses. (C) Refractive index dispersion relations calculated for TE waves of different orders supported by dielectric-metal heterostructures with dielectric layers of different refractive indices. In (B) and (C), the angle of the incident wave was fixed at 45°.

surface of the Si_3N_4 layer). It is known that the separation of electric and magnetic fields in a photonic crystal leads to a small group velocity or the strong localization of electromagnetic wave. It is believed that the spatial separation of electric and magnetic fields in the TE wave is responsible for the large quality factor or the narrow linewidth of the optical mode, as demonstrated later. Since the damping of the electromagnetic wave originates mainly from the imaginary part of the metal (or the oscillation of free electrons in the metal film), the localization of the electric field on the surface of the dielectric layer significantly reduces the propagation loss or the damping rate of the TE wave, leading to a higher quality factor or a narrower linewidth as compared with the TM wave propagating on the surface of bare metal.

However, a careful inspection reveals that the longitudinal component of the magnetic field (H_x) is localized at the interface between the Si_3N_4 layer and the Ag film. The transverse component of the magnetic field (H_z) is localized on the surface of the Si_3N_4 layer. It is remarkable that the enhancement of total electric field of the TM wave (~9.0) is slightly larger than that of the TE wave (~8.0). However, the enhancement factor of the in-plane electric field for the TE wave (E_y) is larger than that for the TM wave (E_x) by a factor of ~3.0. Previously, it was demonstrated that the coupling between the SPPs generated on the surface of a metal film (i.e., TM wave) and the excitons in a two-dimensional material enters into the strong coupling regime [43]. Owing to the enhanced in-plane electric field and the reduced damping rate of the TE wave, it is expected that a stronger interaction between two-dimensional materials and light can be easily realized by using such TE waves.

The resonant wavelength of the TE wave supported by a dielectric-metal heterostructure depends not only on the angle of the excitation light but also on the thickness of the dielectric layer. Basically, the resonant wavelength of a TE wave can be extracted from the calculation of the reflection spectrum. For a Si_3N_4 layer with h = 90 nm, the resonant wavelength of the TE wave can span the entire visible light spectrum (400–720 nm) by simply varying the incidence angle from 44° to 89°, as shown in Figure 3A. One can also extract the dispersion curves for TE waves of different orders by simply increasing the thickness or the refractive index of the dielectric layer, as shown in Figure 3B and C, respectively. In these cases, the angle of the incident wave was fixed at 45°. It is noticed that the resonant wavelength of the TE wave is red shifted from the ultraviolet to the visible spectral range with increasing thickness of the dielectric layer. It enters into the visible light spectrum (λ ~ 380 nm) when the thickness of the Si_3N_4 layer exceeds ~35 nm. It should be emphasized that the critical thickness depends also on the refractive index of the dielectric material. In our case, the critical thickness for the Si_3N_4 is obtained based on the numerical simulation. Physically, it is possible to derive an analytical expression for the critical thickness once the configuration of the dielectric-metal heterostructure is determined. Owing to the large quality factors or narrow linewidths of the TE modes, a small variation in thickness or refractive index can be readily resolved in the reflection spectrum (see Supporting Information, Figure S1), indicating its potential applications in optical sensing, as demonstrated later. It is noticed that the quality factor becomes larger for high-order modes, implying an improved localization or a reduced damping (see Supporting Information, Figure S2). With increasing thickness of the Si_3N_4 layer, it is found that the high-order TM modes with narrow linewidths can also be excited (see Supporting Information, Figures S3–S5).

Basically, the TE and TM waves supported in the Si_3N_4/Ag heterostructure can be excited via the so-called

Kretschmann–Raether configuration by using white light with different incidence angles, as schematically illustrated in Figure 1H. The TE and TM waves can be readily characterized by measuring either the reflection spectra of the incident light or the scattering spectra of polystyrene (PS) nanospheres located on the Si_3N_4 layer. In our experiments, we used PS nanospheres with diameters of ~300 nm, which do not exhibit any optical resonance in the visible light spectrum, to extract the TE and TM waves excited in a Si_3N_4/Ag heterostructure. The scattering light of PS nanospheres was directed to a spectrometer for analysis or to a charge coupled device for imaging. In order to show the advantages of TE waves, we firstly examined the TM waves (i.e., SPPs) generated on the surface of an Ag film, as shown in Figure 4A and C where the reflection and scattering spectra measured for *p*-polarized light are presented. As expected, a blueshift of the resonant wavelength as well as a narrowing of the linewidth is observed in both cases when the incidence angle (θ) is increased. For θ = 46°, the resonant wavelength appears at ~550 nm. However, a linewidth as broad as ~60 nm is observed for this TM wave, implying a severe damping of the amplitude during the propagation. The resonant wavelengths and linewidths extracted from the reflection spectra at different incidence angles are in good agreement with those obtained from the scattering spectra. In Figure 4B and D, we present the reflection and scattering spectra measured for the TE waves generated by using *s*-polarized light (see Supporting Information, Figure S6). Interestingly, it is found that the linewidths for the TE waves are dramatically reduced as compared with those for the TM waves. For instance, a linewidth as narrow as ~10 nm is observed for the lowest-order TE wave at ~550 nm, as shown in Figure 4B and D. This value is reduced by a factor of ~6.0 as compared with that observed for the lowest-order TM wave at the same wavelength (see Figure 4A and C). The narrow linewidths of the TE waves give rise to vivid colors with good chromaticity, as shown in Figure 4E and F. The chromaticity coordinates extracted from the scattering spectra of PS nanospheres are distributed outside the RGB triangle, implying potential applications in high-quality optical display. It is found that colors good chromaticity

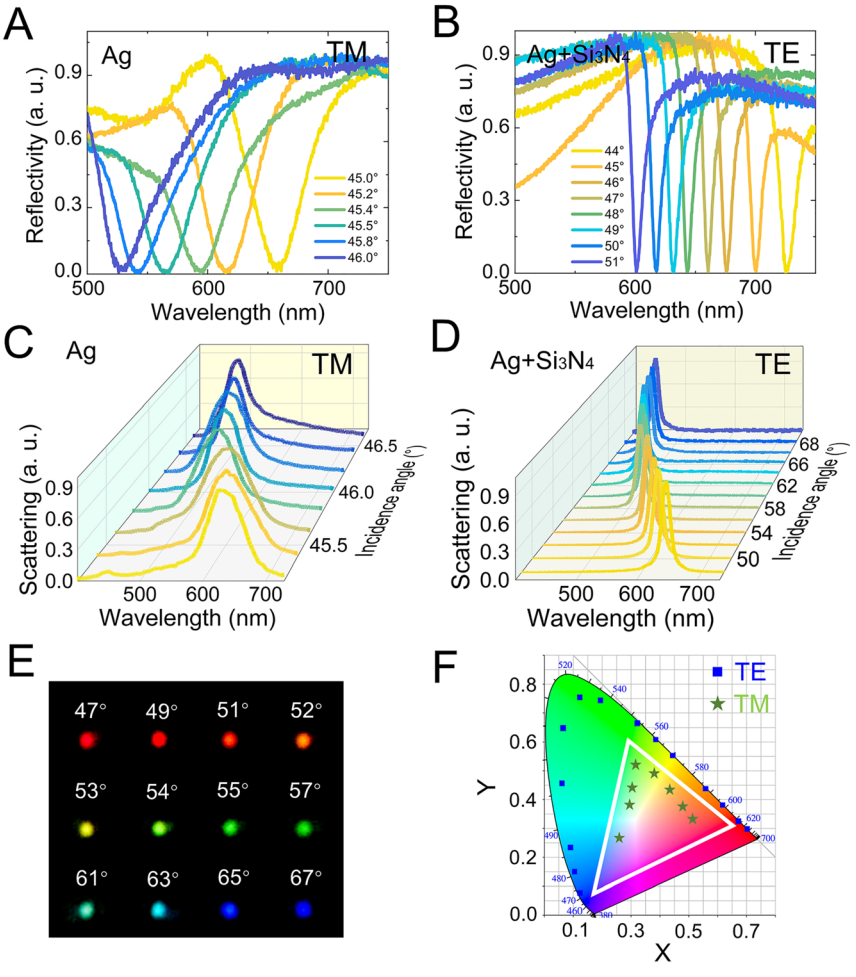

Figure 4: Reflection spectra measured for the lowest-order TM (A) and TE (B) wave excited in a Si_3N_4/Ag heterostructure. The thicknesses of the Si_3N_4 layer and the Ag film were designed to be 100 and 50 nm, respectively. The corresponding scattering spectra are shown in (C) and (D), respectively. (E) CCD images of the scattering light measured the TE waves excited at different incidence angles. (F) Chromaticity coordinates extracted from the scattering spectra of the TE (squares) and TM (stars) waves of the lowest-order excited at different incidence angles.

can also be achieved in high-order TM waves, which possess slightly smaller linewidths as compared with the TE waves of the same order (see Supporting Information, Figure S7).

Since the electric fields of such TE waves are localized in the Si_3N_4 layer, the energy losses of TE waves are significantly suppressed as compared with their counterparts (i.e., SPPs). This unique feature renders them narrow linewidths and small damping rates, which are crucial for practical application in low-loss waveguiding. Actually, the physical mechanism for the excitation of TE waves in a dielectric-metal heterostructure described in this work is completely different from that for the excitation of a hybrid mode in a dielectric-metal waveguide proposed previously. In the latter case, the hybrid mode is formed by the coupling of the dielectric mode and the SPP mode. The electric field is dominated by the component normal to the surfaces of both the dielectric rod and the metal film, quite similar to that in the SPP mode. In addition, the electric field is strongly localized in the gap region between the dielectric rod and the metal film. Finally, the propagation distance of the hybrid mode is only slightly longer than that of the SPP mode. The major advantage of the hybrid mode is the strong localization of the electric field, which was latterly exploited to realize a nanoscale laser [44]. In comparison, the TE waves supported by a dielectric-metal heterostructure contain only the electric field parallel to the surfaces of the dielectric layer and the metal film. The physical mechanism responsible for the small damping rates of TE waves is attributed to the spatial separation of the electric field and the magnetic field. The localization of the electric field on the surface of the dielectric layer leads to a much smaller damping rate and a much longer propagation distance as compared with the SPP mode (i.e., TM waves).

In the experiments described above, PS nanospheres without any resonance in the visible light spectrum were used to scatter the propagating TE waves into far field for nanoscale optical display. In principle, one can design and make nano-antennas with different resonant wavelengths in the dielectric layer (here is Si_3N_4) as the light extractors for TE waves propagating in the dielectric-metal heterostructure. It implies that a nanoscale wavelength demultiplexer can be constructed by using such a dielectric-metal heterostructure with nano-antennas patterned in the dielectric layer. Of course, the structures of nano-antennas must be deliberately designed in order to support optical modes with narrow linewidths. In this work, we simply dug holes in the Si_3N_4 layer by using the combination of electron beam lithography and reactive ion etching and used them to extract the TE waves propagating in the Si_3N_4/Ag heterostructure. In Figure 5A, we show the scanning electron microscopy (SEM) image of the logo of our school, which is composed of an array of nanoholes dug in the Si_3N_4 layer (see Supporting Information, Figure S8). The scattering spectra of a single nanohole measured at

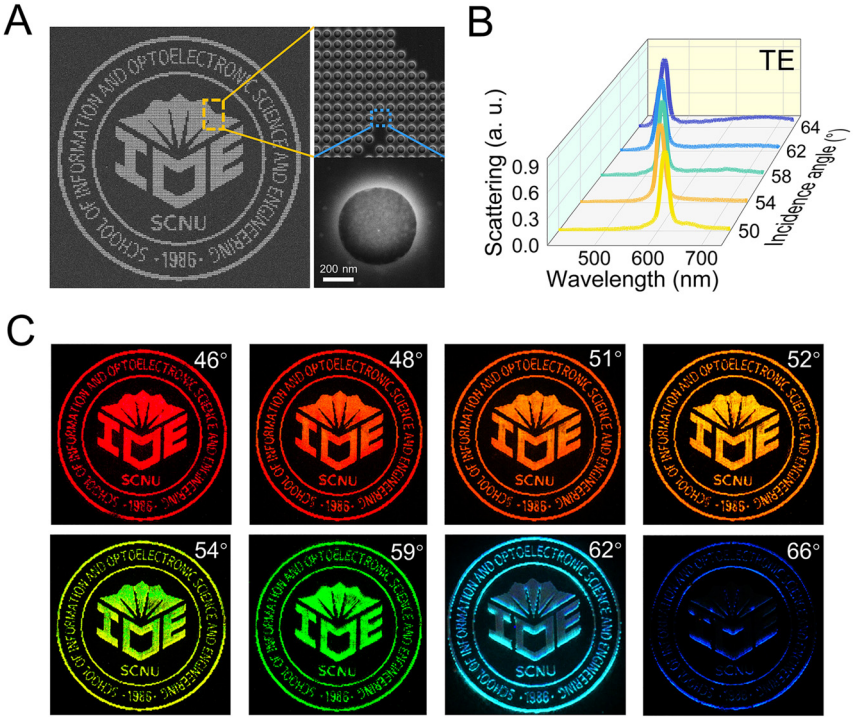

Figure 5: (A) SEM images of the school logo composed of nanoholes dug in the Si_3N_4 layer. (B) Scattering spectra measured at a nanohole used to scatter the TE wave excited at different incidence angles. (C) Color displays of the school logo by using the TE waves excited at different incidence angles and scattered by patterned nanoholes.

different incidence angles are shown in Figure 5B. A blueshift of the scattering peak is observed with increasing incidence angle. As demonstrated in Figure 5C, high-quality color display with a spatial resolution close to the optical diffraction limit (~500 nm) can be realized by exploiting the narrow linewidths of the TE waves excited in the Si_3N_4/Ag heterostructure.

Apart from waveguiding, color display and demultiplexing, the strong dependence of the resonant wavelength on the thickness and refractive index of the dielectric layer, which originates from the large dispersion of the lowest-order TE wave (see Figure 3), can be exploited to construct highly sensitive optical sensors, as demonstrated in the following. Based on numerical simulation, it is revealed that a wavelength shift as large as ~5.0 nm can be achieved in the lower-order TE wave when the thickness of the Si_3N_4 layer is varied by only 1.0 nm. In practice, one can replace Si_3N_4 with a piezoelectric ceramic whose thickness can be readily changed by applying an external voltage. As a result, the resonant wavelength of the TE wave at a specified incidence angle can be modified to span the entire visible light spectrum. It means that an electrically-driven optical display with high spatial resolution and good chromaticity can be implemented by using such a dielectric-metal heterostructure. Here, we demonstrated a highly sensitive optical sensing by exploiting this unique feature of the TE waves. The experimental setup is schematically shown in Figure 6A. In this case, a thin alcohol film was covered on the surface of the Si_3N_4/Ag sample with patterned nanoholes. We chose alcohol because of its rapid evaporation rate in air and large expansion coefficient upon heating. These two features were employed to change the thickness of the thin alcohol film. The resonant wavelength of the TE wave at a specified incidence angle was dictated by the effective thickness of the dielectric layer, which is now the Si_3N_4 layer plus the alcohol film. If we monitored the scattering peak of a nanohole for the TE wave excited at $\theta = 48°$, a gradual blueshift was seen with increasing observation time (see Supporting Information, Figure S9). This blueshift was caused by the gradual evaporation of alcohol in air, which reduces the effective thickness of the dielectric layer. A blueshift of ~5.0 nm was found in the scattering peak after ~300 s, which corresponds to a reduction of ~2.5 nm in the thickness of the alcohol film due to evaporation. Now we lightened an alcohol lamp and moved it close to and away from the sample. The heating of the alcohol film led to the increase of its thickness, as schematically shown in Figure 6B. In this case, a rapid shaking of the scattering peak was detected, as shown in Figure 6C

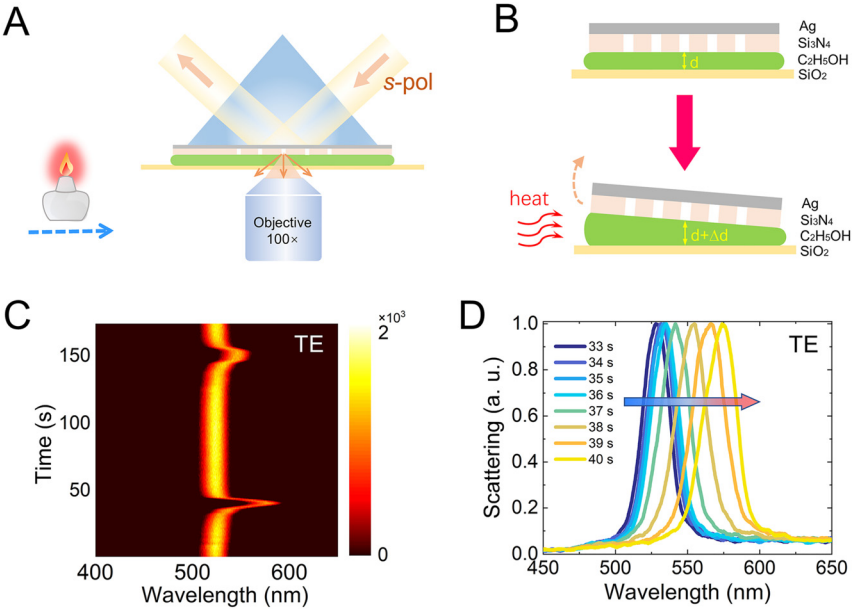

Figure 6: (A) Schematic showing the sensing experiment carried out in this work. The Si_3N_4/Ag heterostructure was covered by an alcohol film and a glass slide. The TE wave supported by the Si_3N_4/Ag heterostructure was excited by *s*-polarized and scattered into far field by a nanohole. An alcohol lamp was moved toward and away from the sample. (B) Schematic showing the expansion of the alcohol film with increasing temperature. (C) Two-dimensional scattering intensity as functions of wavelength and time measured for a Si_3N_4/Ag heterostructure covered with a thin alcohol film. The alcohol lamp was moved close to and away from the sample at ~36 and ~150 s. (D) Evolution of the scattering spectrum observed in a time interval of 33–40 s.

and D. It is suggested that the thermal expansion and thermally-induced refractive index change of the alcohol film, which lead to an increase of the effective thickness of the dielectric layer, are responsible for the redshift of the scattering peak. This behavior was easily reproduced if we repeated the same action, as shown in Figure 6C. Here, the shift of the scattering peak originates from the change in the optical thickness of the alcohol film induced by heating. In this case, both the thickness and the refractive index of the alcohol film are expected to vary when the alcohol film is heated. Although it is difficult to measure such changes, we can estimate the change in the optical thickness of the alcohol film. Based on the dispersion curves of the TE wave, the change in the optical thickness of the alcohol film is calculated to be ~60 nm, corresponding to the wavelength shift of ~40 nm observed in the experiment. It indicates clearly that the TE waves with narrow linewidths and large dispersions can be employed to realize highly sensitive optical sensing. As discussed above, the small damping rate of the TE wave leads to a narrow linewidth of the scattering peak, which implies a high sensitivity in optical sensing. As shown in Figure S1, one can easily discriminate a thickness change as small as ~0.1 nm, which is not easily available by using other methods or instruments. In addition, the thickness change of the dielectric layer is directly reflected in the color change of the scattering light, which is more versatile and convenient for practical sensing applications.

3 Conclusion

In summary, we proposed a dielectric-metal heterostructure supporting TE waves from the viewpoint of optical magnetism and investigated the optical properties of the TE waves propagating in a Si_3N_4/Ag heterostructure. It was found that the thickness of the Si_3N_4 layer must exceed a critical value in order to support the lowest-order TE wave. It was revealed by numerical simulation that the electric fields of TE waves are localized on the surface of the Si_3N_4 layer while the magnetic fields are localized at the interface between the Si_3N_4 layer and the Ag film. This unique feature leads to small damping rates and narrow linewidths for the TE waves. These properties were utilized to realize optical display with high spatial resolution and good chromaticity. Moreover, the lowest-order TE wave exhibits a strong dependence on the thickness and refractive index of the Si_3N_4 layer (i.e., large dispersion) and it was exploited to demonstrate highly sensitive optical sensing. Our findings open new horizons for creating magnetic plasmons in a dielectric-metal heterostructure and pave the way for the practical applications of TE waves in optical waveguiding, display, demultiplexing and sensing.

4 Methods

Sample preparation and characterization

The Si_3N_4 layer used in this work was deposited on a 50-nm-thick Ag film via high-frequency plasma-enhanced chemical vapor deposition (HF-PECVD) method using a gas mixture of SiH_4 and NH_3 as the precursor. The flow rate of SiH_4 and NH_3 were maintained at 3 sccm, 7.5 sccm, respectively. The RF power, deposition pressure, and substrate temperature were set to be 30 W, 60 Pa, and 80 °C, respectively. The thickness of the Si_3N_4 layer could be controlled by the deposition time. The thickness and optical constant of the Si_3N_4 layer were measured by ellipsometry. The nanoholes in the Si_3N_4 layer were created by using the combination of electron beam lithography and reactive ion etching. The morphologies of nanoholes were examined by SEM observation (Gemini 500, Zeiss).

Optical characterization

The reflection spectrum of the Si_3N_4/Ag heterostructure was measured with a spectrometer (USB4000, Ocean Insight). The light scattered from polystyrene (PS) spheres or nanoholes were collected by using the 100× objective lens of an inverted microscope (Axio Observer A1, Zeiss) and directed to a spectrometer (SR-500i-B1, Andor) for analysis or to a charge-coupled device (DU970N, Andor) for imaging.

Numerical simulation

The scattering spectra of the Si_3N_4 cuboids placed on the Ag film, the PS nanospheres placed on the Si_3N_4/Ag heterostructure, and the nanoholes drilled in the Si_3N_4 layer were calculated numerically by using the finite-difference time-domain (FDTD) method (FDTD solution, https://www.lumerical.com). In the numerical simulation, the permittivity of Ag was fitted from the experimental data [45]. The refractive index of Si_3N_4 is based on the measured data. A dipole source oriented along the *y* direction, which was placed at the center of the Si_3N_4 cuboid, was used to excite the eigenmodes of the Si_3N_4 cuboids. In the calculation of the scattering spectra, a total-field scattered-field source polarized along the *x* or *y* direction, which corresponds to *p*- or *s*-polarized light, was obliquely incident on the Si_3N_4/Ag heterostructure. The TE or TM waves scattered by a PS nanospheres or a nanoholes were recorded by six detectors inclosing the PS nanosphere or the nanohole. In the calculation of the reflection spectra, *p*- and *s*-polarized plane waves were used to excite TM and TE waves supported by Si_3N_4/Ag heterostructures. In all numerical simulations, the smallest mesh of 1.0 nm was used in order to obtain converged simulation results and perfectly matched layer boundary condition was employed to terminate the finite simulation region.

Acknowledgment: S. Lan acknowledges the financial support from the National Key Research and Development

Program of China (No. 2016YFA0201002), the National Natural Science Foundation of China (Grant Nos. 11674110 and 11874020), and the Science and Technology Program of Guangzhou (No. 2019050001).

Author contribution: All the authors have accepted responsibility for the entire content of this submitted manuscript and approved submission.

Research funding: The study was financially supported by National Key Research and Development Program of China (No. 2016YFA0201002); National Natural Science Foundation of China (Grant Nos. 11674110 and 11874020); Science and Technology Program of Guangzhou (No. 2019050001).

Conflict of interest statement: The authors declare no conflicts of interest regarding this article.

References

[1] R. Ritchie, "Surface plasmons in solids," *Surf. Sci.*, vol. 34, pp. 1–19, 1973.

[2] E. Kretschmann, "Die Bestimmung optischer Konstanten von Metallen durch Anregung von Oberflächenplasmaschwingungen," *E. Z. Phys.*, vol. 241, pp. 313–324, 1971.

[3] H. Raether, "Surface plasmons on smooth surfaces," in *Surface plasmons on smooth and rough surfaces and on gratings*, Springer, 1988, pp. 4–39.

[4] B. Hecht, H. Bielefeldt, L. Novotny, Y. Inouye, and D. Pohl, "Local excitation, scattering, and interference of surface plasmons," *Phys. Rev. Lett.*, vol. 77, p. 1889, 1996.

[5] G. Di Martino, Y. Sonnefraud, S. Kéna-Cohen, et al., "Quantum statistics of surface plasmon polaritons in metallic stripe waveguides," *Nano Lett.*, vol. 12, pp. 2504–2508, 2012.

[6] S. I. Bozhevolnyi, V. S. Volkov, E. Devaux, and T. W. Ebbesen, "Channel plasmon-polariton guiding by subwavelength metal grooves," *Phys. Rev. Lett.*, vol. 95, p. 046802, 2005.

[7] J. N. Anker, W. P. Hall, O. Lyandres, N. C. Shah, J. Zhao, and R. P. Van Duyne, "Biosensing with plasmonic nanosensors," in *Nanoscience and Technology: A Collection of Reviews from Nature Journals*, World Scientific, 2010, pp. 308–319.

[8] L. Guo, J. A. Jackman, H.-H. Yang, P. Chen, N.-J. Cho, and D.-H. Kim, "Strategies for enhancing the sensitivity of plasmonic nanosensors," *Nano Today*, vol. 10, pp. 213–239, 2015.

[9] M. A. Schmidt, D. Y. Lei, L. Wondraczek, V. Nazabal, and S. A. Maier, "Hybrid nanoparticle–microcavity-based plasmonic nanosensors with improved detection resolution and extended remote-sensing ability," *Nat. Commun.*, vol. 3, pp. 1–8, 2012.

[10] M. A. Otte, B. Sepulveda, W. Ni, J. P. Juste, L. M. Liz-Marzán, and L. M. Lechuga, "Identification of the optimal spectral region for plasmonic and nanoplasmonic sensing," *ACS Nano*, vol. 4, pp. 349–357, 2010.

[11] M. Noginov, G. Zhu, M. Mayy, B. Ritzo, N. Noginova, and V. Podolskiy, "Stimulated emission of surface plasmon polaritons," *Phys. Rev. Lett.*, vol. 101, p. 226806, 2008.

[12] M. I. Stockman, "Spasers explained," *Nat. Photonics*, vol. 2, pp. 327–329, 2008.

[13] S. I. Azzam, A. V. Kildishev, R.-M. Ma, et al., "Ten years of spasers and plasmonic nanolasers," *Light Sci. Appl.*, vol. 9, pp. 1–21, 2020.

[14] R. H. Ritchie, "Plasma losses by fast electrons in thin films," *Phys. Rev.*, vol. 106, p. 874, 1957.

[15] W. L. Barnes, A. Dereux, and T. W. Ebbesen, "Surface plasmon subwavelength optics," *Nature*, vol. 424, pp. 824–830, 2003.

[16] J. B. Khurgin, "How to deal with the loss in plasmonics and metamaterials," *Nat. Nanotechnol.*, vol. 10, pp. 2–6, 2015.

[17] P. Berini, "Surface plasmon photodetectors and their applications," *Laser Photon. Rev.*, vol. 8, pp. 197–220, 2014.

[18] N. Kroo, J.-P. Thost, M. Völcker, W. Krieger, and H. Walther, "Decay length of surface plasmons determined with a tunnelling microscope," *Europhys. Lett.*, vol. 15, p. 289, 1991.

[19] A. Bouhelier, T. Huser, H. Tamaru, et al., "Plasmon optics of structured silver films," *Phys. Rev. B*, vol. 63, p. 155404, 2001.

[20] J. Seidel, S. Grafström, and L. Eng, "Stimulated emission of surface plasmons at the interface between a silver film and an optically pumped dye solution," *Phys. Rev. Lett.*, vol. 94, p. 177401, 2005.

[21] I. V. Smetanin, A. Bouhelier, and A. V. Uskov, "Coherent surface plasmon amplification through the dissipative instability of 2D direct current," *Nanophotonics*, vol. 8, pp. 135–143, 2018.

[22] I. De Leon and P. Berini, "Amplification of long-range surface plasmons by a dipolar gain medium," *Nat. Photonics*, vol. 4, pp. 382–387, 2010.

[23] H. Zhang, J. Zhou, W. Zou, and M. He, "Surface plasmon amplification characteristics of an active three-layer nanoshell-based spaser," *J. Appl. Phys.*, vol. 112, p. 074309, 2012.

[24] P. Berini and I. De Leon, "Surface plasmon–polariton amplifiers and lasers," *Nat. Photonics*, vol. 6, pp. 16–24, 2012.

[25] J. Pitarke, V. Silkin, E. Chulkov, and P. Echenique, "Theory of surface plasmons and surface-plasmon polaritons," *Rep. Prog. Phys.*, vol. 70, p. 1, 2006.

[26] T. Ma and G. Shvets, "All-Si valley-Hall photonic topological insulator," *New J. Phys.*, vol. 18, p. 025012, 2016.

[27] A. Lagarkov, I. Boginskaya, I. Bykov, et al., "Light localization and SERS in tip-shaped silicon metasurface," *Opt. Express*, vol. 25, pp. 17021–17038, 2017.

[28] J. Tian, H. Luo, Q. Li, X. Pei, K. Du, and M. Qiu, "Near-infrared super-absorbing all-dielectric metasurface based on single-layer germanium nanostructures," *Laser Photon. Rev.*, vol. 12, p. 1800076, 2018.

[29] Y. Yang, N. Kamaraju, S. Campione, et al., "Transient GaAs plasmonic metasurfaces at terahertz frequencies," *ACS Photonics*, vol. 4, pp. 15–21, 2017.

[30] S. Wang, Z.-L. Deng, Y. Wang, et al., "Arbitrary polarization conversion dichroism metasurfaces for all-in-one full Poincaré sphere polarizers," *Light Sci. Appl.*, vol. 10, pp. 1–9, 2021.

[31] J. Xiang, J. Li, Z. Zhou, et al., "Manipulating the orientations of the electric and magnetic dipoles induced in silicon nanoparticles for multicolor display," *Laser Photon. Rev.*, vol. 12, p. 1800032, 2018.

[32] H. Li, Y. Xu, J. Xiang, et al., "Exploiting the interaction between a semiconductor nanosphere and a thin metal film for nanoscale plasmonic devices," *Nanoscale*, vol. 8, pp. 18963–18971, 2016.

[33] J. J. Mock, R. T. Hill, A. Degiron, S. Zauscher, A. Chilkoti, and D. R. Smith, "Distance-dependent plasmon resonant coupling between a gold nanoparticle and gold film," *Nano Lett.*, vol. 8, pp. 2245–2252, 2008.
[34] I. Sinev, I. Iorsh, A. Bogdanov, et al., "Polarization control over electric and magnetic dipole resonances of dielectric nanoparticles on metallic films," *Laser Photon. Rev.*, vol. 10, pp. 799–806, 2016.
[35] E. Xifre-Perez, L. Shi, U. Tuzer, et al., "Mirror-image-induced magnetic modes," *ACS Nano*, vol. 7, pp. 664–668, 2013.
[36] A. K. Sarychev, G. Shvets, and V. M. Shalaev, "Magnetic plasmon resonance," *Phys. Rev. E*, vol. 73, p. 036609, 2006.
[37] G. T. Papadakis, A. Davoyan, P. Yeh, and H. A. Atwater, "Mimicking surface polaritons for unpolarized light with high-permittivity materials," *Phys. Rev. Mater.*, vol. 3, p. 015202, 2019.
[38] G. T. Papadakis, D. Fleischman, A. Davoyan, P. Yeh, and H. A. Atwater, "Optical magnetism in planar metamaterial heterostructures," *Nat. Commun.*, vol. 9, pp. 1–9, 2018.
[39] N. C. Passler, A. Heßler, M. Wuttig, T. Taubner, and A. Paarmann, "Surface polariton-like s-polarized waveguide modes in switchable dielectric thin films on polar crystals," *Adv. Opt. Mater.*, vol. 8, p. 1901056, 2020.
[40] F. L. Riley, "Silicon nitride and related materials," *J. Am. Ceram. Soc.*, vol. 83, pp. 245–265, 2000.
[41] H. R. Philipp, "Optical properties of silicon nitride," *J. Electrochem. Soc.*, vol. 120, p. 295, 1973.
[42] Z.-L. Deng, X. Ye, H.-Y. Qiu, et al., "Full-visible transmissive metagratings with large angle/wavelength/polarization tolerance," *Nanoscale*, vol. 12, pp. 20604–20609, 2020.
[43] F. Deng, H. Liu, L. Xu, S. Lan, and A. E. Miroshnichenko, "Strong exciton–plasmon coupling in a WS2 monolayer on Au film hybrid structures mediated by liquid Ga nanoparticles," *Laser Photon. Rev.*, vol. 14, p. 1900420, 2020.
[44] R. F. Oulton, V. J. Sorger, D. Genov, D. Pile, and X. Zhang, "A hybrid plasmonic waveguide for subwavelength confinement and long-range propagation," *Nat. Photonics*, vol. 2, pp. 496–500, 2008.
[45] P. B. Johnson and R.-W. Christy, "Optical constants of the noble metals," *Phys. Rev. B*, vol. 6, p. 4370, 1972.

Supplementary Material: The online version of this article offers supplementary material (https://doi.org/10.1515/nanoph-2021-0146).